CHEMISTRY OF MATERIALS
Article

Chem. Mater. **2010,** *22,* 2573–2581 2573
DOI:10.1021/cm903616d

Synthesis of Multicomponent Olivine by a Novel Mixed Transition Metal Oxalate Coprecipitation Method and Electrochemical Characterization

Young-Uk Park, Jongsoon Kim, Hyeokjo Gwon, Dong-Hwa Seo, Sung-Wook Kim, and Kisuk Kang*

Department of Materials Science and Engineering and KAIST Institute for Eco-Energy, KAIST, Gwahangno 335, Yuseong-gu, Daejeon, Korea 305-701

Received November 30, 2009. Revised Manuscript Received February 11, 2010

The multicomponent olivine cathode material, $LiMn_{1/3}Fe_{1/3}Co_{1/3}PO_4$, was prepared via a novel coprecipitation method of the mixed transition metal oxalate, $Mn_{1/3}Fe_{1/3}Co_{1/3}(C_2O_4)\cdot 2H_2O$. The stoichiometric ratio and distribution of transition metals in the oxalate, therefore, in the olivine product, was affected sensitively by the environments in the coprecipitation process, while they are the important factors in determining the electrochemical property of electrode materials with multiple transition metals. The effect of the pH, atmosphere, temperature, and aging time was investigated thoroughly with respect to the atomic ratio of transition metals, phase purity, and morphology of the mixed transition metal oxalate. The electrochemical activity of each transition metal in the olivine synthesized through this method clearly was enhanced as indicated in the cyclic voltammetry (CV) and galvanostatic charge/discharge measurement. Three distinctive contributions from Mn, Fe, and Co redox couples were detected reversibly in multiple charge and discharge processes. The first discharge capacity at the *C*/5 rate was 140.5 mAh g^{-1} with good cycle retention. The rate capability test showed that the high capacity still is retained even at the 4*C* and 6*C* rates with 102 and 81 mAh g^{-1}, respectively.

1. Introduction

The advanced lithium rechargeable battery technology is vital in realizing hybrid electric vehicle (HEV), plug-in hybrid electric vehicle (PHEV), and electric vehicle (EV) applications in our daily lives.[1,2] Most of all, the key issue in the lithium rechargeable batteries lies in developing reliable electrode materials with high performance and low cost. The current choice of the cathode material, $LiCoO_2$, has been studied extensively since the 1970s.[3] Despite its wide usage, the desire for cheaper, safer, and better-performing cathode materials led to the development of similar layered compounds with multiple transition metals substituting Co.[4−9] One of the most well-known multicomponent layered oxides is $LiNi_{1/3}Mn_{1/3}Co_{1/3}O_2$.[10] Unlike single-component layered oxides, each transition metal in this compound has unique roles when substituted homogeneously in the structure; where the Ni^{2+}/Ni^{4+} redox couple mainly contributes to the high capacity, Mn^{4+} acts as a structural stabilizer, and Co^{3+} ensures a layered structure preventing cation disorder, thereby enhancing the electrochemical property of layered compounds.[1,11,12] However, the electrochemical performance of $LiNi_{1/3}Mn_{1/3}Co_{1/3}O_2$ was affected strongly by synthesis conditions, depending on which the distribution of transition metals in the host structure varies significantly.[13] The local segregation of each transition metal in the layered structure can cause various problems related to each single-transition metal layered compound. To ensure the homogeneity of transition metal distribution in a layered structure, many process methods have been suggested,[8,14−16] among which the coprecipitation of mixed transition metal hydroxides or carbonates has been proven to be an effective way to synthesize multicomponent layered compounds with good electrochemical properties.

*To whom correspondence should be addressed. E-mail: matlgen1@kaist.ac.kr. Tel: +82-42-350-3341. Fax: +82-42-350-3310.

(1) Kang, K.; Meng, Y. S.; Breger, J.; Grey, C. P.; Ceder, G. *Science* **2006**, *311*, 977–980.
(2) Armand, M.; Tarascon, J. M. *Nature* **2008**, *451*, 652–657.
(3) Whittingham, M. S. *Chem. Rev.* **2004**, *104*, 4271–4302.
(4) Liu, Z.; Yu, A.; Lee, J. Y. *J. Power Sources* **1999**, *81−82*, 416–419.
(5) Yoshio, M.; Noguchi, H.; Itoh, J.-i.; Okada, M.; Mouri, T. *J. Power Sources* **2000**, *90*, 176–181.
(6) Ohzuku, T.; Makimura, Y. *Chem. Lett.* **2001**, *30*, 642–643.
(7) Lu, Z.; MacNeil, D. D.; Dahn, J. R. *Electrochem. Solid-State Lett.* **2001**, *4*, A191–A194.
(8) Yabuuchi, N.; Ohzuku, T. *J. Power Sources* **2003**, *119−121*, 171–174.
(9) Choi, J.; Manthiram, A. *Electrochem. Solid-State Lett.* **2004**, *7*, A365–A368.
(10) Li, D.-C.; Muta, T.; Zhang, L.-Q.; Yoshio, M.; Noguchi, H. *J. Power Sources* **2004**, *132*, 150–155.
(11) Reed, J.; Ceder, G. *Electrochem. Solid-State Lett.* **2002**, *5*, A145–A148.
(12) Hwang, B. J.; Tsai, Y. W.; Carlier, D.; Ceder, G. *Chem. Mater.* **2003**, *15*, 3676–3682.
(13) Cho, T.-H.; Shiosaki, Y.; Noguchi, H. *J. Power Sources* **2006**, *159*, 1322–1327.
(14) Kosova, N. V.; Devyatkina, E. T.; Kaichev, V. V. *J. Power Sources* **2007**, *174*, 735–740.
(15) Zhang, Y.; Cao, H.; Zhang, J.; Xia, B. *Solid State Ionics* **2006**, *177*, 3303–3307.
(16) Paulsen, J. M.; Dahn, J. R. *J. Electrochem. Soc.* **2000**, *147*, 2478–2485.

Published on Web 03/10/2010

Recently, $LiMPO_4$ (M = Mn, Fe, Co, or Ni) with olivine structure has been studied widely as a new cathode material for lithium rechargeable batteries because of their low cost, low environmental impact, and safety.[17,18] In particular, $LiFePO_4$[19] and $LiMnPO_4$[20,21] are being explored most vigorously. More recently, multicomponent olivine cathode materials[22−27] also are getting attention because of their promising properties such as enhanced energy density or increased rate capability over its single component counterpart. The theoretical and experimental study on $LiMn_{1/3}Fe_{1/3}Co_{1/3}PO_4$ demonstrated that (i) Mn activity, when it is present with Fe and Co in the olivine, is significantly enhanced, and (ii) Fe and Co redox potentials increase and decrease, respectively, in favor of practical usage.[22] Furthermore, unexpected one-phase based Li intercalation/deintercalation reaction was observed in the olivine framework.[22] We believe that these unique properties would be sensitively dependent on the distribution of transition metals in the structure. In this work, we prepare a mixed transition metal precursor in the form of oxalate, which is the most frequently used precursor in olivine synthesis, via a novel coprecipitation method to promote homogeneous mixing of transition metals. We find that the controls of pH, atmosphere, temperature, and aging time are very important in obtaining a stoichiometric, homogeneously mixed transition metal oxalate precursor due to the differences in chemical behaviors of Fe, Co, and Mn ions. The electrochemical properties of $LiMn_{1/3}Fe_{1/3}Co_{1/3}PO_4$ synthesized from coprecipitated oxalate are shown to be remarkably better not only than those of our previously reported hydrothermally synthesized $LiMn_{1/3}Fe_{1/3}Co_{1/3}PO_4$[22] but also than those of a standard sample prepared using conventional individual transition metal oxalates.

2. Experimental Section

2.1. Preparation of a Mixed Transition Metal Oxalate. A number of mixed transition metal oxalates, $Mn_{1/3}Fe_{1/3}Co_{1/3}(C_2O_4)\cdot 2H_2O$, were prepared in different coprecipitation conditions using various precursors of transition metal ions and oxalic ions for the study. For the sample SO, sulfate sources of $MnSO_4\cdot H_2O$ (99%, Aldrich), $FeSO_4\cdot 7H_2O$ (99%, Aldrich), $CoSO_4\cdot 7H_2O$ (99%, Aldrich), and oxalic acid ($H_2C_2O_4\cdot 2H_2O$, 99%, Aldrich) with a molar ratio of 1:1:1:3 were used. For the sample AO, acetate sources of $Mn(CH_3COO)_2\cdot 4H_2O$ (97%, Junsei), $Fe(CH_3COO)_2$ (95%, Aldrich), $Co(CH_3COO)_2\cdot 4H_2O$ (99%, Aldrich), and oxalic acid ($H_2C_2O_4\cdot 2H_2O$, 99%, Aldrich) with a molar ratio of 1:1:1:3 were used. For the sample SA1, SA2, and SA3, sulfate sources of $MnSO_4\cdot H_2O$ (99%, Aldrich), $(NH_4)_2Fe(SO_4)_2\cdot 6H_2O$ (99%, Aldrich), $CoSO_4\cdot 7H_2O$ (99%, Aldrich), and ammonium oxalate ($(NH_4)_2C_2O_4\cdot H_2O$, 99%, Aldrich) with a molar ratio of 1:1:1:3 were used. We prepared two different aqueous solutions: (i) 0.7 M mixed transition metal sulfate (SO, SA1, SA2, and SA3) or acetate (AO only) solution and (ii) 0.5 M oxalic acid (SO and AO) or ammonium oxalate (SA1, SA2, and SA3) solution. The former was added to the latter dropwise with stirring. The coprecipitation reaction was continued for 2 h in the ambient air (SO, AO, and SA1) or in Ar-filled glovebox (SA2 and SA3). The temperature of a reaction bath was maintained at 25 °C (SO, AO, SA1, and SA2) or 90 °C (SA3 only), and the coprecipitated solution was aged in an Ar atmosphere for 1 h (SO, AO, SA1, and SA2) or 7 h (SA3 only). The differences in synthesis conditions among samples are tabulated in Table 1. After precipitation and cooling, the precipitate was separated and washed with DI water by centrifugal separation using a multipurpose centrifuge (Hanil Science Industrial, HA 1000−6, Korea) at room temperature. The centrifugal separation was carried out three times (5 min per each time) at 4000 rpm. The separated precipitate was dried at 70 °C in a vacuum oven for 10 h.

Table 1. Various Coprecipitation Conditions (M^{2+} Source, $C_2O_4^{2-}$ Source, Atmosphere, Temperature, Aging Time, and pH)

sample name	M^{2+} source	$C_2O_4^{2-}$ source	atmosphere	temperature (°C)	aging time (h)
SO	sulfate	oxalic acid	air	25	1
AO	acetate	oxalic acid	air	25	1
SA1	sulfate	ammonium oxalate	air	25	1
SA2	sulfate	ammonium oxalate	Ar	25	1
SA3	sulfate	ammonium oxalate	Ar	90	7

$MnC_2O_4\cdot 2H_2O$ (Mn 30% min, Alfa Aesar), $FeC_2O_4\cdot 2H_2O$ (99%, Aldrich), $CoC_2O_4\cdot 2H_2O$ (Reagent grade, Alfa Aesar), H_2SO_4 (95%, Junsei), and CH_3COOH (99%, Junsei) were used to test the solubility of oxalates at various pH conditions (Figure 1). We prepared three different solutions by dissolving about 130 mg of each $MC_2O_4\cdot 2H_2O$ (M = Mn, Fe, or Co) in DI water. To these solutions, 1 mL of sulfuric acid (Figure 1a), 0.14 mL of sulfuric acid (Figure 1b), or 1 mL of acetic acid (Figure 1c) was added, keeping the total solution volume equal to 5 mL. As a result, nine different solutions were prepared. The pH and the concentration of a solution in Figure 1b are equivalent to the synthesis condition of the sample SO.

2.2. Preparation of $LiMn_{1/3}Fe_{1/3}Co_{1/3}PO_4$. The multicomponent olivine $LiMn_{1/3}Fe_{1/3}Co_{1/3}PO_4$ was synthesized by a solid-state reaction using LiH_2PO_4 (97%, Alfa Aesar) and the mixed transition metal oxalate, $Mn_{1/3}Fe_{1/3}Co_{1/3}(C_2O_4)\cdot 2H_2O$, prepared in section 2.1 with a molar ratio of 1:1. Pyromellitic acid hydrate, 6 wt % (PA, 99%, Fluka), was added as an organic additive. The mixture was wet ball-milled using acetone for 18 h. After evaporation of the acetone, the mixture was heated at 500 °C for 10 h under Ar flow. The calcined sample was cooled to room temperature and reground. Additionally, 6 wt % PA as an organic additive and 1 wt % ferrocene (98%, Aldrich) as a graphitization catalyst were added to carbon-coat the material. This whole mixture was ball-milled again in acetone media for 2 h. After evaporation of the acetone, the mixture was pelletized

(17) Padhi, A. K.; Nanjundaswamy, K. S.; Goodenough, J. B. *J. Electrochem. Soc.* **1997**, *144*, 1188–1194.
(18) Yamada, A.; Hosoya, M.; Chung, S.-C.; Kudo, Y.; Hinokuma, K.; Liu, K.-Y.; Nishi, Y. *J. Power Sources* **2003**, *119−121*, 232–238.
(19) Ellis, B. L.; Makahnouk, W. R. M.; Makimura, Y.; Toghill, K.; Nazar, L. F. *Nat. Mater.* **2007**, *6*, 749–753.
(20) Li, G.; Azuma, H.; Tohda, M. *Electrochem. Solid-State Lett.* **2002**, *5*, A135–A137.
(21) Kim, S.-W.; Kim, J.; Gwon, H.; Kang, K. *J. Electrochem. Soc.* **2009**, *156*, A635–A638.
(22) Gwon, H.; Seo, D.-H.; Kim, S.-W.; Kim, J.; Kang, K. *Adv. Funct. Mater.* **2009**, *19*, 3285–3292.
(23) Zhang, Y.; Sun, C. S.; Zhou, Z. *Electrochem. Commun.* **2009**, *11*, 1183–1186.
(24) Kuo, H. T.; Chan, T. S.; Bagkar, N. C.; Liu, G. Q.; Liu, R. S.; Shen, C. H.; Shy, D. S.; Xing, X. K.; Chen, J. M. *J. Phys. Chem. B* **2008**, *112*, 8017–8023.
(25) Chen, J.; Vacchio, M. J.; Wang, S.; Chernova, N.; Zavalij, P. Y.; Whittingham, M. S. *Solid State Ionics* **2008**, *178*, 1676–1693.
(26) Wang, X. J.; Yu, X. Q.; Li, H.; Yang, X. Q.; McBreen, J.; Huang, X. J. *Electrochem. Commun.* **2008**, *10*, 1347–1350.
(27) Nam, K.-W.; Wang, X.-J.; Yoon, W.-S.; Li, H.; Huang, X.; Haas, O.; Bai, J.; Yang, X.-Q. *Electrochem. Commun.* **2009**, *11*, 913–916.

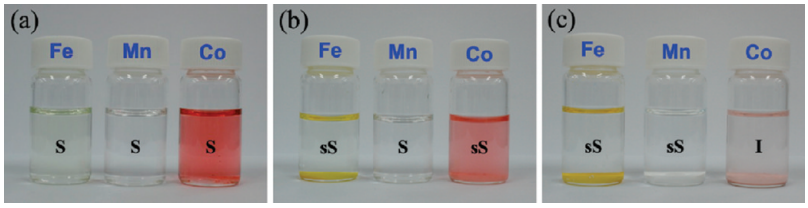

Figure 1. Variation of the solubility of each $MC_2O_4 \cdot 2H_2O$ (M = Mn, Fe, or Co) with the pH. About 130 mg of each $MC_2O_4 \cdot 2H_2O$ was dissolved in DI water. After the addition of (a) 1 mL of sulfuric acid, (b) 0.14 mL of sulfuric acid, and (c) 1 mL of acetic acid, more DI water was added to make the total solution volume equal 5 mL. The resulting pH was (a) −0.5, (b) 0.5, and (c) 2.2. This experiment was conducted under air. S = soluble, sS = slightly soluble, I = insoluble.

manually under 200 kg cm^{-2} pressure using a disk-shape mold. The pellet was heated again at 600 °C for 10 h under Ar flow, cooled to room temperature, and finally ground. To obtain a standard data, another batch of $LiMn_{1/3}Fe_{1/3}Co_{1/3}PO_4$ was prepared using exact same procedure except only the type of the transition metal sources. For this standard sample, individual transition metal oxalates, $MnC_2O_4 \cdot 2H_2O$ (Mn 30% min, Alfa Aesar), $FeC_2O_4 \cdot 2H_2O$ (99%, Aldrich), and $CoC_2O_4 \cdot 2H_2O$ (Reagent grade, Alfa Aesar), were used as the transition metal sources instead of the mixed transition metal oxalate, $Mn_{1/3}Fe_{1/3}Co_{1/3}(C_2O_4) \cdot 2H_2O$, prepared in section 2.1.

2.3. Sample Characterization. The pH of various solutions was measured using a pH meter (Thermo Scientific Orion 2-Star pH benchtop meter, Thermo Electron Corporation, MA) equipped with a puncture combination electrode (ROSS Ultra pH/ATC Triode, Thermo Electron Corporation, MA). Thermal gravimetric analysis (TGA) and differential scanning calorimetry (DSC) were performed under a nitrogen atmosphere at a heating rate of 10 °C min^{-1} using a Setsys16/18 thermogravimetry analyzer (SETARAM, France) from room temperature to 600 °C. The atomic ratio of various elements such as Li, Mn, Fe, Co, and P in a mixed transition metal oxalate, and $LiMn_{1/3}Fe_{1/3}Co_{1/3}PO_4$ was determined by inductively coupled plasma atomic emission spectroscopy (ICP-AES, Thermo Jarrel Ash, Polyscan 60E, U.S.). The content of carbon in samples was measured by a carbon−sulfur determinator (ELTRA CS-800, Germany). The content of oxygen in samples was determined by an oxygen−nitrogen−hydrogen determinator (ELTRA ONH-2000, Germany). Investigation of the crystal structure was carried out using an X-ray diffractometer (XRD, Rigaku, D/MAX-RB diffractometer, Tokyo, Japan) equipped with Cu Kα radiation by step scanning (0.01° s^{-1}) in the 2θ range of 10−70° for a mixed transition metal oxalate and 10−85° for $LiMn_{1/3}Fe_{1/3}Co_{1/3}PO_4$. Structural refinements were performed by the Rietveld method using the Fullprof software.[28] The size and morphology of the powdered samples were observed using a field emission scanning electron microscope (FE-SEM, Philips, XL30 FEG, Eindhoven, Netherlands). The infrared spectra of $LiMn_{1/3}Fe_{1/3}Co_{1/3}PO_4$ in the range from 1300 to 400 cm^{-1} were recorded with an FT-IR spectrometer (Jasco, FR/IR-4100, Japan) using the KBr pellet technique.

2.4. Electrochemical Tests. For the electrochemical characterization, a slurry of 79 wt % $LiMn_{1/3}Fe_{1/3}Co_{1/3}PO_4$, 12 wt % carbon black, and 9 wt % polyvinylidene fluoride (PVDF) dispersed in *N*-methyl-2-pyrrolidone (NMP) was prepared and casted on aluminum foils using a doctor-blade. NMP was evaporated at 110 °C for 2 h under air. Electrochemical cells were assembled into a CR2016 type coin-cell with Li counter electrode, separator (Celgard 2400), and 1 M solution of $LiPF_6$ in a mixture of ethyl carbonate/dimethyl carbonate (EC/DMC, 1:1 v/v) in an Ar-filled glovebox. The cyclic voltammetry (CV) and the galvanostatic charge/discharge test was carried out between 2.0 and 4.9 V at room temperature using a potentiogalvanostat (WonA Tech, WBCS 3000, Korea). The CV measurement was performed at a scan rate of 0.02 mV s^{-1}. Cells were cycled with either constant current (CC) mode or constant current constant voltage (CCCV) mode. The galvanostatic charge/discharge test was carried out at various *C* rates (6*C*, 4*C*, 2*C*, 1*C*, *C*/2, and *C*/5). 1*C* corresponds to 169 mA g^{-1}.

3. Results and Discussion

3.1. Factors That Affect the Properties of a Mixed Transition Metal Oxalate. We performed coprecipitation experiments with various conditions of M^{2+} and $C_2O_4^{2-}$ sources, pH, atmosphere, temperature, and aging time. The detailed conditions and corresponding samples are summarized in Table 1. The careful analysis of samples was done to accurately characterize their properties.

3.1.1. Effect of pH. We started our experiment of coprecipitation with metal sulfates and oxalic acid, which are the most conventionally used precursors for the synthesis of iron oxalates.[29] The coprecipitation occurred as the mixed metal sulfate solution was added to the oxalic acid solution dropwise. The obtained coprecipitated sample (SO) was under ICP-AES analysis. Unexpectedly, significant Mn deficiency (20.4 at. % vs target 33.3 at. %) was observed as shown in Table 2. To determine the origin of Mn deficiency in the SO, we investigated the effect of pH on the stoichiometry of the mixed transition metal oxalate by conducting the dissolution and the solubility experiment of each metal oxalate in a separate experimental setup.

Figure 1 shows the variation of the solubility of each $MC_2O_4 \cdot 2H_2O$ (M = Mn, Fe, or Co) with varying pH. At a pH of 0.5 (Figure 1b), which is equivalent to that in the synthesis condition of SO, it is clear that $MnC_2O_4 \cdot 2H_2O$ is soluble in water, while $FeC_2O_4 \cdot 2H_2O$ and $CoC_2O_4 \cdot 2H_2O$ are only slightly soluble. Further experiments show that $MnC_2O_4 \cdot 2H_2O$ is completely soluble at very low pH (Figure 1a) and only slightly soluble at pH 2.2 (Figure 1c). $FeC_2O_4 \cdot 2H_2O$ is completely dissolved immediately in the solution at pH −0.5 (Figure 1a). However, $FeC_2O_4 \cdot 2H_2O$ is only slightly dissolved in the solution at pH 0.5 (Figure 1b) and pH 2.2 (Figure 1c). $CoC_2O_4 \cdot 2H_2O$ is completely soluble at pH −0.5 (Figure 1a), slightly

(28) Roisnel, T.; Rodríguez-Carvajal, J. *Mater. Sci. Forum* **2001**, *378−381*, 118–123.

(29) Suresh, P.; Shukla, A. K.; Munichandraiah, N. *J. Power Sources* **2006**, *159*, 1395–1400.

soluble at pH 0.5 (Figure 1b), and insoluble at pH 2.2 (Figure 1c). These variations of the solubility in water could be recognized easily by observing the color of solutions and the amount of powder on the bottom of vials remaining undissolved in DI water qualitatively. For example, the color of $CoC_2O_4 \cdot 2H_2O$ solution is dark pink when completely dissolved because of the Co^{2+} ions (Figure 1a), pale pink when slightly dissolved (Figure 1b), and colorless when no dissolution of Co^{2+} ions occurs (Figure 1c). This simple qualitative experiment indicates that the Mn deficiency in the mixed transition metal oxalate is most likely caused by the high tendency for Mn dissolution in the low pH condition of the coprecipitating solution. The pH of the remaining solution after the coprecipitation was measured to be about 0.5 in the preparation of SO. The Mn dissolution will be much more prevalent than Fe and Co dissolution, as we observed that $MnC_2O_4 \cdot 2H_2O$ is more soluble than $FeC_2O_4 \cdot 2H_2O$ and $CoC_2O_4 \cdot 2H_2O$ under the low pH condition of the experiments ($\sim$0.5).

Using metal acetate sources instead of metal sulfate sources could result in a milder condition of acidity in the process, since the remaining solution after precipitation is more like acetic acid than sulfuric acid. As indicated in Table 2, the AO sample prepared from metal acetate sources shows significant improvement in meeting the targeted stoichiometry of transition metals. The Mn ratio increased from 20 to 30 at. % close to the targeted 33.3 at. %. However, a slight deficiency of Mn is still observed. This is most likely the result of the still low pH of the synthesis condition, even when using acetate (pH $\sim$2.2 measured). Figure 1c shows that Mn and Fe are slightly soluble even at pH $\sim$2.2, while Co is not. In the case of the sample SO, because the remaining solution after coprecipitation is sulfuric acid, the pH of the solution decreases remarkably during the reaction ($\sim$0.5), while that of the AO is the weak acetic acid. To increase pH further, we used ammonium oxalate instead of oxalic acid as precursors, which resulted in the pH value of $\sim 4.5 \pm 0.5$. The atomic percentage of Mn in this sample of SA1 approached the targeted value (33.1 at.%). However, in this case, although the Mn dissolution problem was nearly solved, a slight Fe deficiency was observed, as shown in Table 2. The color of the remaining solution after the reaction was observed to be yellow in the case of SA1, which implies that some transition metal ions are still dissolved in the solution.

A low pH condition plays two opposite roles in getting the stoichiometric oxalate: (i) it accelerates the dissolution of transition metals in the solution, causing off-stoichiometry, and (ii) it prevents transition metal ions, especially Fe^{2+} ions, from being oxidized.[30] Figure 1a shows that the color of $FeC_2O_4 \cdot 2H_2O$ solution is pale green, which is the typical color of Fe^{2+} ions in water solution. While Fe^{2+} ions get easily oxidized to Fe^{3+} ions in ambient water conditions, this indicates that the low pH condition prevented the Fe^{2+} ions from being oxidized to Fe^{3+} ions. Since the oxidation state of metal in the targeted oxalate is +2, it is important that the metal ions should be kept at 2+ in the event of coprecipitation. Since the pH condition of SA1 ($\sim 4.5 \pm 0.5$) becomes significantly high, the oxidation of Fe^{2+} ions to Fe^{3+} ions is likely to occur to some extent. The yellow color of the remaining solution of SA1 (not shown here) is additional evidence of the presence of Fe^{3+} ions. Note that the color of a dilute solution containing hydrated iron(III) ions, $[Fe^{3+}(H_2O)_6]$ (aq), is yellow, and the color of an iron(III) oxalate complex, $[Fe^{3+}(C_2O_4^{2-})_3]$ (aq), is also yellow.[31] The partial oxidation of Fe^{2+} to Fe^{3+} will result in the deficiency of Fe^{2+} that precipitates with $C_2O_4^{2-}$. The Fe^{3+} is likely to form iron(III) complexes, $[Fe^{3+}(H_2O)_6]$ (aq) or $[Fe^{3+}(C_2O_4^{2-})_3]$ (aq), that do not participate in the precipitation. Therefore, the stoichiometric mixed transition metal oxalate is barely achieved solely by controlling the pH condition.

Table 2. Atomic Percents of Transition Metals in Mixed Transition Metal Oxalates Obtained from ICP-AES Measurements

sample name	Mn	Fe	Co
SO	20.4	38.3	41.3
AO	30.1	32.8	37.1
SA1	33.1	31.4	35.5
SA2	32.3	34.1	33.6
SA3	32.5	34.1	33.4
theoretical value[a]	33.3	33.3	33.3

[a] This value was calculated from the weight percent of each transition metal (Mn, Fe, and Co) in $Mn_{1/3}Fe_{1/3}Co_{1/3}(C_2O_4) \cdot 2H_2O$.

3.1.2. Effect of Atmosphere. At a relatively high pH condition, Fe^{2+} ions get easily oxidized to Fe^{3+} ions under the existence of water and oxygen dissolved in water. Because the water is necessary for coprecipitation reactions, we attempted to remove the oxygen as much as possible in the synthesis to prevent the oxidation of Fe^{2+}. Using the same metal and oxalic sources with those used for the SA1 preparation, the SA2 sample was synthesized in the Ar-filled glovebox instead of in the ambient air. The resultant SA2 was under careful ICP-AES analysis. Table 2 shows that the transition metal ratio among Mn, Fe, and Co now has become 1.00:1.05:1.04, close to the targeted ratio indicating that the problem of Fe deficiency has been resolved.

The SA2 was also subject to the XRD analysis to check the phase purity of the oxalate. Figure 2a shows the XRD patterns of the SA2. The observed peak patterns match the sets of XRD peaks from typical oxalate phases. However, it appears that the α and β phases of oxalate coexist. It is mostly the β-oxalate phase but with a trace of α-oxalate.

3.1.3. Effect of Temperature and Aging Time. Deyrieux et al. reported that $FeC_2O_4 \cdot 2H_2O$[32] and $CoC_2O_4 \cdot 2H_2O$[33] have temperature-dependent polymorphisms.

(30) Balmer, M. E.; Sulzberger, B. *Environ. Sci. Technol.* **1999**, *33*, 2418–2424.

(31) Flinn Scientific, Inc. Publication No. 571.00. http://www.flinnsci.com/Documents/demoPDFs/Chemistry/CF0571.00.pdf (accessed November **2009**).

(32) Deyrieux, R.; Peneloux, A. *Bull. Soc. Chim. Fr.* **1969**, 2675–&.

(33) Deyrieux, R.; Berro, C.; Peneloux, A. *Bull. Soc. Chim. Fr.* **1973**, 25–34.

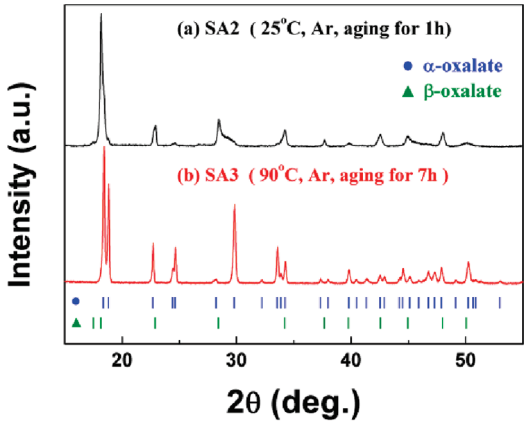

Figure 2. XRD patterns of $Mn_{1/3}Fe_{1/3}Co_{1/3}(C_2O_4)\cdot 2H_2O$ synthesized by the coprecipitation method. (a) SA2 (25 °C, Ar, aging for 1 h) and (b) SA3 (90 °C, Ar, aging for 7 h). The observed peak positions of α- and β-oxalates are denoted as blue bars (●) and green bars (▲), respectively.

One is monoclinic α-oxalate (space group 15, *C2/c*),[34] and the other is orthorhombic β-oxalate (space group 66, *Cccm*). In an α-oxalate structure, all metal ions are located in symmetrically equivalent sites, while in a β-oxalate structure, metal ions are located in two different sites as a result of the reduction of the symmetry.[32−34] There are two major differences between α- and β-oxalates in XRD patterns. A main peak around $2\theta = 18.5°$ splits into two clear peaks in α-oxalate, while it maintains a single peak in β-oxalate. Also, peaks around $2\theta = 24.5°$ are appreciable in α-oxalate but negligible in β-oxalate.[32,33] In contrast to $FeC_2O_4\cdot 2H_2O$ and $CoC_2O_4\cdot 2H_2O$, the temperature-dependent polymorphism of $MnC_2O_4\cdot 2H_2O$ is not reported.[33] $MnC_2O_4\cdot 2H_2O$ is always in the monoclinic α-oxalate phase. Therefore, the fact that SA2 is a mixture of α- and β-oxalates implies that the composition of transition metals can be significantly different in each polymorphism. It is very likely to have a mixture of Mn-deficient β-oxalate and Mn-rich α-oxalate. This will result in a nonhomogeneous distribution of the transition metals in the final product.

It was reported that the α-oxalate (Fe or Co) typically is obtained at 90 °C with aging of some time, while the β-oxalate (Fe or Co) is obtained at room temperature.[32,33] In Figure 2a, a single main peak around $2\theta = 18.5°$ and only a small shoulder peak around $2\theta = 18.84°$ indicates that the main phase is β-oxalate with a trace amount of α-oxalate in SA2. This is because $FeC_2O_4\cdot 2H_2O$ and $CoC_2O_4\cdot 2H_2O$ are stable at the β-phase in room temperature synthesis, while $MnC_2O_4\cdot 2H_2O$ is not.[32−34] For this reason, the temperature and aging time were controlled to yield only the α-phase oxalate where all of the transition metals (Fe, Co, and Mn) may be energetically stable. By performing the coprecipitation at 90 °C with aging of 7 h, the SA3 sample was obtained using the same precursors of SA2. Figure 2b shows that a main peak around $2\theta = 18.5°$ clearly splits into two peaks for SA3 and that no peak from the β-phase is observable, implying that a pure α-oxalate phase was obtained. More conclusive evidence is shown in Figure 3 and Table 3 with Rietveld refinement of the XRD pattern, which will be discussed in section 3.2.

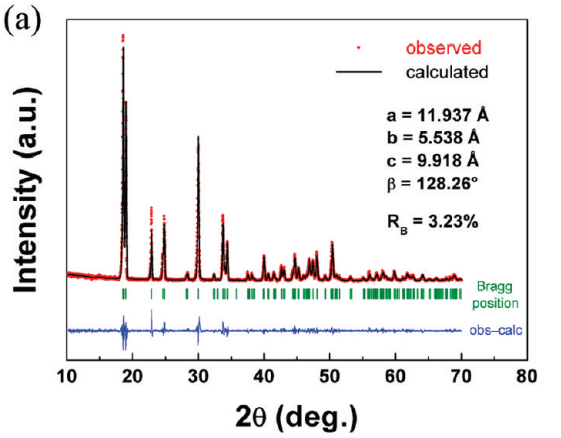

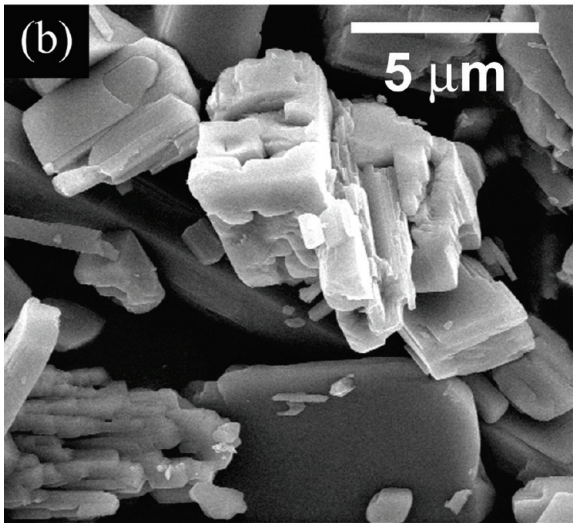

Figure 3. (a) XRD pattern and Rietveld refinement using space group *C2/c* and (b) SEM image of sample SA3.

3.2. Characterization of a Mixed Transition Metal Oxalate (Sample SA3). Figure 3a shows the XRD pattern and Rietveld refinement results of SA3. The Rietveld refinement was performed using space group *C2/c* with a monoclinic unit cell. The lattice parameters obtained from the refinement are tabulated in Table 3 in comparison to the reported lattice parameters of each α-$MC_2O_4\cdot 2H_2O$ (M = Mn, Fe, or Co). The lattice parameters of SA3 are $a = 11.937$ Å, $b = 5.538$ Å, $c = 9.918$ Å, $\beta = 128.26°$, and $V = 514.822$ Å^3. These numbers are very close to the average value of the lattice parameters of each α-$MC_2O_4\cdot 2H_2O$ (M = Mn, Fe, or Co), implying that the transition metals are mixed homogeneously in the structure. The SEM image of SA3 in Figure 3b shows that its average particle size is about 5 μm. The shape of the particles resembles a typical morphology of α-oxalate crystals with a monoclinic unit cell, as Angermann and Töpfer reported.[34]

Figure 4 shows the TGA/DSC curves for the mixed transition metal oxalate. There are two weight-losing endothermic steps observed. The first decomposition step is attributed to a dehydration process or the loss of crystal

(34) Angermann, A.; Töpfer, J. *J. Mater. Sci.* **2008**, *43*, 5123–5130.

Table 3. Lattice Constants of SA3 Obtained from Rietveld Refinement and Each α-$MC_2O_4 \cdot 2H_2O$ (M = Mn, Fe, or Co)

	a (Å)	*b* (Å)	*c* (Å)	*β* (°)	*V* (Å^3)
SA3[a]	11.937	5.538	9.918	128.26	514.822[b]
α-$MnC_2O_4 \cdot 2H_2O$[33]	12.016	5.632	9.961	128.40	528.289
α-$FeC_2O_4 \cdot 2H_2O$[34]	11.998	5.546	9.900	128.59	514.902
α-$CoC_2O_4 \cdot 2H_2O$[33]	11.775	5.416	9.859	127.90	496.130

[a] In this work. [b] This value is very close to the average value of the unit cell volume of each α-$MC_2O_4 \cdot 2H_2O$ (M = Mn, Fe, or Co), which is 513.107 Å^3.

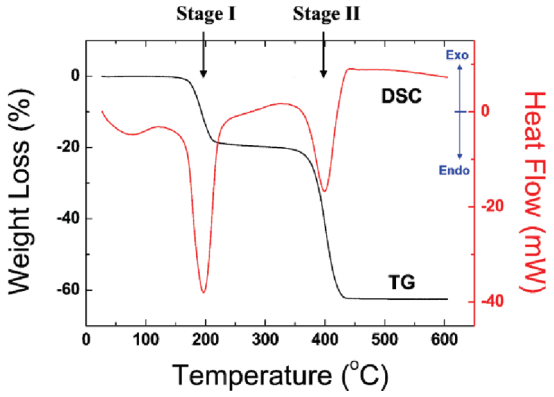

Figure 4. Thermal decomposition of $Mn_{1/3}Fe_{1/3}Co_{1/3}(C_2O_4) \cdot 2H_2O$ (SA3) in nitrogen. Heating rate 10 °C min^{-1}. In a DSC curve, the dehydration process of each $MC_2O_4 \cdot 2H_2O$ (M = Mn, Fe, or Co) occurs simultaneously in the same temperature range.

water molecules from the mixed transition metal oxalates. The next one is likely to be a decomposition process to metal oxide or metal. In the TGA curve, the ratio of weight loss in the first step, which is attributed to the dehydration process, was about 19.8%. The theoretical weight loss of the dehydration process of $MC_2O_4 \cdot 2H_2O$ (M = Mn, Fe, or Co) is 20.12%, 20.0%, and 19.68%, respectively.[35] Considering the atomic ratio of transition metals, the weight loss of $Mn_{1/3}Fe_{1/3}Co_{1/3}(C_2O_4) \cdot 2H_2O$ is calculated to be 19.93%. We observe that the measured weight loss of SA3 of 19.8% is close to the expected value. According to the DSC curve, the first weight loss is accompanied by a sharp endothermic peak (196.5 °C). The dehydration process is the endothermic reaction as follows:

$$Mn_{1/3}Fe_{1/3}Co_{1/3}(C_2O_4) \cdot 2H_2O \rightarrow Mn_{1/3}Fe_{1/3}Co_{1/3}(C_2O_4) + 2H_2O\uparrow$$

Even though it has been reported that the dehydration process (stage I) of each $MC_2O_4 \cdot 2H_2O$ (M = Mn, Fe, or Co) occurs at significantly different temperature ranges, as shown in Table 4,[36−40] only one sharp endothermic peak is observed in the DSC curve for the SA3. This is further evidence that the transition metals are homogeneously mixed in the oxalate structure.

The second step is the decomposition to metal oxide or metal. In the TGA curve, the second weight loss is about 42.65%. The reported reactions of the decomposition process of anhydrous MC_2O_4 (M = Mn, Fe, or Co) in an inert atmosphere (nitrogen or helium) are as follows:[36−40]

$$MnC_2O_4\ (s) \rightarrow MnO\ (s) + CO\ (g)\uparrow + CO_2\ (g)\uparrow \quad (\text{theoretical weight loss} = 40.24\%)$$

$$4FeC_2O_4\ (s) \rightarrow Fe_3O_4\ (s) + Fe\ (s) + 4CO\ (g)\uparrow + 4CO_2\ (g)\uparrow \quad (\text{theoretical weight loss} = 40.03\%)$$

$$CoC_2O_4\ (s) \rightarrow Co\ (s) + 2CO_2\ (g)\uparrow \quad (\text{theoretical weight loss} = 48.11\%)$$

Considering the atomic ratio of transition metals, the weight loss of the decomposition process of anhydrous $Mn_{1/3}Fe_{1/3}Co_{1/3}(C_2O_4)$ is likely to be 42.79%, which is close to the measured weight loss of SA3 (42.65%). The endothermic weight loss (stage II) is attributed to the decomposition of the anhydrous $Mn_{1/3}Fe_{1/3}Co_{1/3}(C_2O_4)$ into each metal oxide or metal.

3.3. Characterization of $LiMn_{1/3}Fe_{1/3}Co_{1/3}PO_4$. Figure 5a shows the XRD pattern and Rietveld refinement of $LiMn_{1/3}Fe_{1/3}Co_{1/3}PO_4$ prepared using SA3 precursor. Good crystalline $LiMn_{1/3}Fe_{1/3}Co_{1/3}PO_4$ was obtained without any trace of impurities or second phases. The Rietveld refinement was performed using space group *Pnma* for an olivine structure with an orthorhombic unit cell. The lattice parameters of $LiMn_{1/3}Fe_{1/3}Co_{1/3}PO_4$ are a = 10.326 Å, b = 6.011 Å, c = 4.713 Å, and V = 292.534 Å^3. These values are very close to the average lattice parameters of each $LiMPO_4$ (M = Fe, Mn, or Co) and are in good agreement with previously reported values.[22,23,25] The SEM image in Figure 5b shows that the average particle size of $LiMn_{1/3}Fe_{1/3}Co_{1/3}PO_4$ is about 100 nm with a spherical shape.

Figure 6 shows the FT-IR spectrum of the olivine $LiMn_{1/3}Fe_{1/3}Co_{1/3}PO_4$. The absorption of FT-IR spectra originates from the intramolecular vibration of the $(PO_4)^{3-}$ unit. There is a broad maximum at 940−1120 and 540−650 cm^{-1} ranges, which can be attributed to P−O vibrations of the $(PO_4)^{3-}$ polyanion.[41,42] The absorption at 1141 cm^{-1} originates from the symmetric and antisymmetric stretching vibrations of O−P−O.[41,43] The absorption at 1059, 1096, 982, and 641 cm^{-1} originate from P−O stretching vibrations.[41] The absorption at 578, 550, and 471 cm^{-1} originate from antisymmetric and symmetric bending vibrations of O−P−O.[41] The

(35) Pan, Y.; Guan, X.; Feng, Z.; Wu, Y.; Li, X. *J. Therm. Anal. Calorim.* **1999**, *55*, 877–884.
(36) Dollimore, D.; Griffiths, D. L. *J. Therm. Anal. Calorim.* **1970**, *2*, 229–250.
(37) Davar, F.; Mohandes, F.; Salavati-Niasari, M. *Inorg. Chim. Acta* **2009**, *362*, 3663–3668.
(38) Nicholson, G. C. *J. Inorg. Nucl. Chem.* **1967**, *29*, 1599–1604.
(39) Hermanek, M.; Zboril, R.; Mashlan, M.; Machala, L.; Schneeweiss, O. *J. Mater. Chem.* **2006**, *16*, 1273–1280.
(40) Majumdar, S.; Sharma, I. G.; Bidaye, A. C.; Suri, A. K. *Thermochim. Acta* **2008**, *473*, 45–49.
(41) Zhang, P.; Li, X.; Luo, Z.; Huang, X.; Liu, J.; Xu, Q.; Ren, X.; Liang, X. *J. Alloys Compd.* **2009**, *467*, 390–396.
(42) Nyquist, R. A.; Kagel, R. O. *Infrared Spectra of Inorganic Compounds (3800−45 cm^{-1})*; Academic Press: New York, 1997.
(43) Chang, C.-C.; Chen, T.-K. *J. Power Sources* **2009**, *193*, 834–840.

Table 4. Temperature Range and Theoretical Weight Losses of Two Different Thermal Decomposition Reactions for Each α-$MC_2O_4 \cdot 2H_2O$ (M = Mn, Fe, or Co) in Nitrogen Atmosphere

		$MnC_2O_4 \cdot 2H_2O$[36,37]	$FeC_2O_4 \cdot 2H_2O$[38,39]	$CoC_2O_4 \cdot 2H_2O$[36,40]
stage I	reaction	endothermic dehydration to produce anhydrous oxalates		
	temperature range	112−131 °C	161−196 °C	149−197 °C
	theoretical weight loss	20.12%	20.0%	19.68%
stage II	reaction	endothermic decomposition to produce metal oxide or metal		
	temperature range	343−396 °C	315−364 °C	355−371 °C
	theoretical weight loss	40.24%	40.03%	48.11%

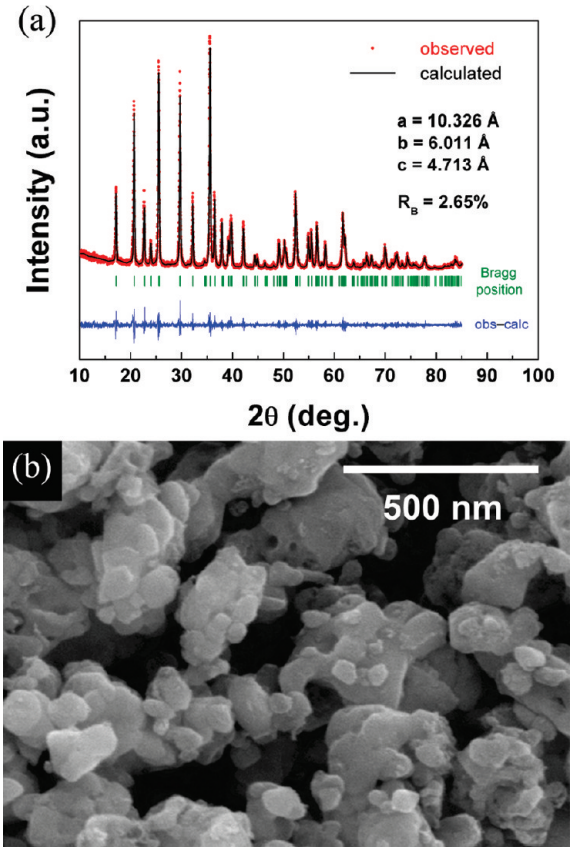

Figure 5. (a) XRD pattern and Rietveld refinement using space group *Pnma* and (b) SEM image of $LiMn_{1/3}Fe_{1/3}Co_{1/3}PO_4$ prepared using SA3 precursor.

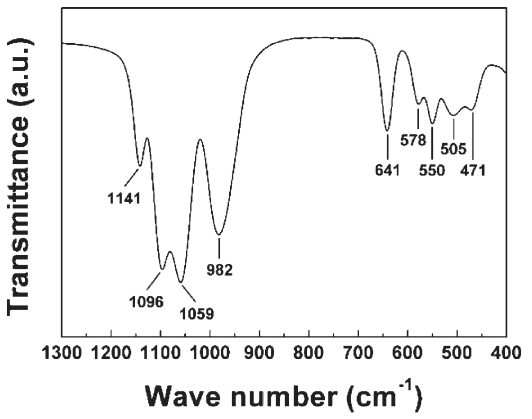

Figure 6. FT-IR spectra of $LiMn_{1/3}Fe_{1/3}Co_{1/3}PO_4$ prepared using SA3 precursor.

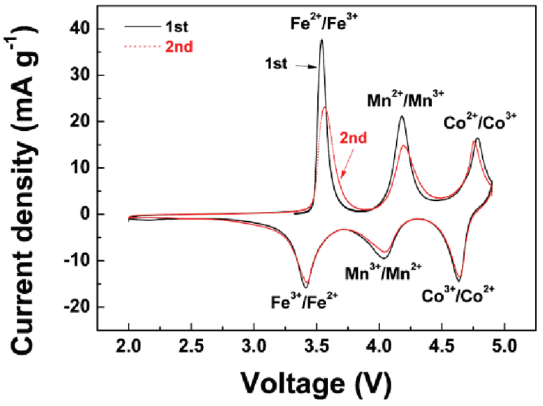

Figure 7. CV measurement for $LiMn_{1/3}Fe_{1/3}Co_{1/3}PO_4$ at scan rate of 0.02 mV s^{-1}.

absorption at 505 cm^{-1} originates from a perturbation bending vibration of O−P−O.[41]

We carried out the ICP-AES measurement and elemental analysis (EA) to confirm the accurate chemical formula of the multicomponent olivine. The atomic ratio of Li, Mn, Fe, Co, and P measured by ICP-AES measurement determined that the Mn/Fe/Co ratio is 0.323:0.344:0.333. The atomic ratio of oxygen and the residual carbon amount determined by an oxygen−nitrogen−hydrogen determinator and a carbon−sulfur determinator showed that the actual chemical formula is $LiMn_{0.323}Fe_{0.344}Co_{0.333}PO_4$ with a carbon content of 2.2 wt %.

3.4. Electrochemical Characterization. Figure 7 shows the cyclic voltammetry (CV) of $LiMn_{1/3}Fe_{1/3}Co_{1/3}PO_4$. There are three distinct peaks in each anodic and cathodic scan. These correspond to three different redox couples: Fe^{2+}/Fe^{3+}, Mn^{2+}/Mn^{3+}, and Co^{2+}/Co^{3+}.[22] The redox potential of Fe^{2+}/Fe^{3+}, Mn^{2+}/Mn^{3+}, and Co^{2+}/Co^{3+} was 3.50 V, 4.13 V, and 4.70 V, respectively. When we compare these potentials with the average redox potentials of pure $LiFePO_4$, $LiMnPO_4$, and $LiCoPO_4$, we can easily notice that considerable voltage shifts occurred in case of the Fe^{2+}/Fe^{3+} and Co^{2+}/Co^{3+} redox couples, while no voltage shift was observed for the Mn^{2+}/Mn^{3+} redox couple. The average value of the charge and the discharge redox potential of Fe^{2+}/Fe^{3+} in $LiMn_{1/3}Fe_{1/3}Co_{1/3}PO_4$ (~3.5 V) were higher than that of Fe^{2+}/Fe^{3+} in pure $LiFePO_4$ (~3.4 V),[44,45] and that of Co^{2+}/Co^{3+} in $LiMn_{1/3}Fe_{1/3}Co_{1/3}PO_4$ (~4.7 V) was lower than that of Co^{2+}/Co^{3+} in pure $LiCoPO_4$ (~4.9 V),[46,47] but that of Mn^{2+}/Mn^{3+} in $LiMn_{1/3}Fe_{1/3}Co_{1/3}PO_4$ (~4.1 V) was

(44) Yamada, A.; Chung, S. C.; Hinokuma, K. *J. Electrochem. Soc.* **2001**, *148*, A224–A229.
(45) Liao, X.-Z.; Ma, Z.-F.; Wang, L.; Zhang, X.-M.; Jiang, Y.; He, Y.-S. *Electrochem. Solid-State Lett.* **2004**, *7*, A522–A525.
(46) Amine, K.; Yasuda, H.; Yamachi, M. *Electrochem. Solid-State Lett.* **2000**, *3*, 178–179.
(47) Eftekhari, A. *J. Electrochem. Soc.* **2004**, *151*, A1456–A1460.

almost the same as that of Mn^{2+}/Mn^{3+} in pure $LiMnPO_4$ (~4.1 V).[20] This trend of voltage shifts of the Fe^{2+}/Fe^{3+} and Co^{2+}/Co^{3+} redox couples is in good agreement with our previous report.[22] Seo et al. reported that the redox potential of each transition metal could shift as a result of charge redistribution, change in the covalency between each transition metal and oxygen causing the inductive effect, and the relative energy change from the multiple M/Li interactions.[48] The detailed theoretical investigation on these is described in reference 48.

Figure 8a shows the galvanostatic charge/discharge curves of $LiMn_{1/3}Fe_{1/3}Co_{1/3}PO_4$ measured at the *C*/5 rate (CCCV mode). Three different potential plateaus related with Fe, Mn, and Co were observed clearly in the first cycle. They are reversibly exhibited even after multiple cycles. In the first cycle, $LiMn_{1/3}Fe_{1/3}Co_{1/3}PO_4$ delivers a discharge capacity of 140.5 mAh g^{-1} (theoretical value is 169 mAh g^{-1}). This value is significantly higher than the previously reported capacity of the same material of about 100 mAh g^{-1} in the same charge/discharge protocol.[22] Also, the 4.1 V plateau, which is attributed to Mn^{2+}/Mn^{3+}, is clearly developed, while it was barely observed in the previous report.[22] This indicates that Mn activity was improved significantly by our coprecipitation synthesis method. However, the capacity decreases to 80.0 mAh g^{-1} in the 20th cycle (Figure 8b). The rate of the capacity fade was rather pronounced. We found that a change in the charge protocol from CCCV mode to CC mode improves the cyclability significantly. A cell charged up to 4.9 V without a constant 4.9 V charging mode retains 88% of initial capacity in the 20th cycle. The noticeable improvement of the capacity retention was obtained simply by changing a charge protocol. This implies that the electrolyte instability when exposed to high potential (4.9 V) for a prolonged time may play a major role in the capacity fade. We expect that the capacity retention can be improved further by the development of an electrolyte that is stable at a high potential.

The rate capability of $LiMn_{1/3}Fe_{1/3}Co_{1/3}PO_4$ obtained using the coprecipitated mixed oxalate (MO-$LiMn_{1/3}Fe_{1/3}Co_{1/3}PO_4$) is shown in Figure 8c (top). For comparison, we also show that of $LiMn_{1/3}Fe_{1/3}Co_{1/3}PO_4$ synthesized using the conventional individual oxalates (IO-$LiMn_{1/3}Fe_{1/3}Co_{1/3}PO_4$) in Figure 8c (bottom). We performed the galvanostatic discharge test for these two samples at various *C* rates (6*C*, 4*C*, 2*C*, 1*C*, *C*/2, and *C*/5). MO-$LiMn_{1/3}Fe_{1/3}Co_{1/3}PO_4$ shows a reasonable capacity of 102 and 81 mAh g^{-1} even at 4*C* and 6*C*, respectively, while IO-$LiMn_{1/3}Fe_{1/3}Co_{1/3}PO_4$ shows a relatively poor capacity of 40 and 32 mAh g^{-1} at same rates. The three distinct potential plateaus in the discharge profile exist clearly up to the 1*C* rate, and they are still observable even at the 4*C* rate in MO-$LiMn_{1/3}Fe_{1/3}Co_{1/3}PO_4$, as shown in Figure 8c (top). However, IO-$LiMn_{1/3}Fe_{1/3}Co_{1/3}PO_4$ exhibits much less distinct potential plateaus than MO-$LiMn_{1/3}Fe_{1/3}Co_{1/3}PO_4$ at same *C* rates. The potential

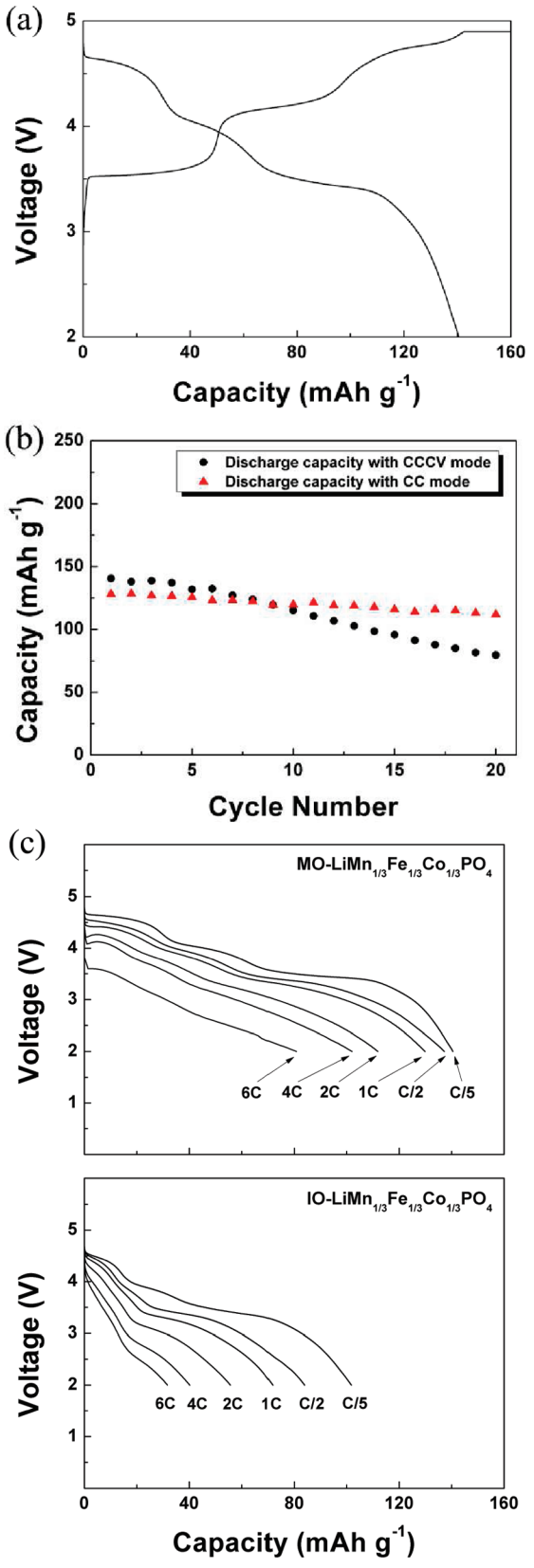

Figure 8. (a) Galvanostatic charge/discharge curves of the first cycle for $LiMn_{1/3}Fe_{1/3}Co_{1/3}PO_4$ between 4.9 and 2 V at a *C*/5 rate. (b) Corresponding cyclability data with two different charge protocols. (c) The discharge curves at various *C* rates (6*C*, 4*C*, 2*C*, 1*C*, *C*/2, and *C*/5) for $LiMn_{1/3}Fe_{1/3}Co_{1/3}PO_4$ from mixed oxalate (MO-$LiMn_{1/3}Fe_{1/3}Co_{1/3}PO_4$, top) and $LiMn_{1/3}Fe_{1/3}Co_{1/3}PO_4$ from individual oxalates (IO-$LiMn_{1/3}Fe_{1/3}Co_{1/3}PO_4$, bottom). In the rate test, the cell was charged at *C*/20 to 4.9 V and discharged to 2.0 V at different rates. 1*C* corresponds to 169 mA g^{-1}.

(48) Seo, D.-H.; Gwon, H.; Kim, S.-W.; Kim, J.; Kang, K. *Chem. Mater.* **2010**, *22*, 518–523.

plateau related to Mn^{3+}/Mn^{2+} redox couple is no more pronounced at the 2*C*, 4*C*, and 6*C* rate for IO-$LiMn_{1/3}Fe_{1/3}Co_{1/3}PO_4$ (bottom). This clearly indicates that the transition metal homogeneity plays an important role in enhancing the Mn activity. The weakening of the Mn plateau is most pronounced among three plateaus, implying that Mn activity is affected significantly by synthesis routes. Because the major drawback of Mn-containing olivine compounds is the sluggish kinetics of the Mn^{2+}/Mn^{3+} redox reaction, the exhibited good rate capability is attributed mainly to the improved Mn activity through the mixed transition metal oxalate coprecipitation method. We believe that this enhanced Mn activity can be ascribed to the improved homogeneity of transition metals in the structure preventing the formation of Mn-rich regions, which will behave similarly to the low rate-capable $LiMnPO_4$.

4. Conclusion

Factors that affect the properties of the mixed transition metal oxalate in a coprecipitation reaction were investigated systematically. We found that the pH/atmosphere affects the atomic ratio of transition metals; the temperature/aging time affects the crystal structure/phase purity of the mixed transition metal oxalate. The mixed transition metal oxalate of a pure phase with accurate stoichiometry was obtained successfully with careful control of factors. Accordingly, the multicomponent olivine compound also was successfully synthesized. Since the properties of the mixed transition metal compounds are sensitively affected by the stoichiometry and the distribution of introduced components, the systematic approach to prepare a mixed transition metal precursor of good quality is critically important.

The obtained multicomponent olivine cathode material exhibited superior electrochemical performance. The first discharge capacity was about 140 mAh g^{-1} at a *C*/5 rate. The rate test showed that the high capacity still remained even at the 4*C* and 6*C* rates with 102 and 81 mAh g^{-1}, respectively. In particular, it was observed that the electrochemical activity of Mn was improved significantly, mainly contributing to the high capacity and good rate capability. We believe that the enhanced Mn activity can be attributed to the homogeneous distribution of transition metals in the olivine structure.

Acknowledgment. This research was supported by the Korea Science & Engineering Foundation (KOSEF) grant (WCU program, 31-2008-000-10055-0) funded by the Ministry of Education and Science & Technology (MEST), the Korea Science and Engineering Foundation (KOSEF) grant funded by the Korea government (MEST) (R11-2008-058-01003-0), the Converging Research Center Program through the National Research Foundation of Korea (NRF) funded by the Ministry of Education, Science and Technology (No. 2009-0082069), and the National Research Foundation of Korea Grant funded by the Korean Government (MEST) (NRF-2009-0094219). This work was also supported by Energy Resources Technology R&D program (20092020100040) under the Ministry of Knowledge Economy, Republic of Korea.